Estimating the energy source and reflectivity by seismic inversion

Susan E. Minkoff and William W. Symes

The Rice Inversion Project, Department of Computational and Applied Mathematics, Rice University, P.O. Box 1892, Houston TX 77251-1892

Short Title: Seismic inversion for the source and reflectivity
Classification numbers: 260, 270, 4360, 9130
Keywords: Acoustic wave propagation, source estimation, seismology

ABSTRACT

Data produced by a reproducible source contains redundant information which allows seismic inversion to simultaneously determine the high-frequency fluctuation in the P-wave velocity (or reflectivity) as well as the input energy source. The seismogram model is the plane-wave convolutional model derived from the constant density, variable sound velocity acoustic wave equation. The first step is to analyze this linearized model when the background velocity is constant. Then perturbations in the seismic data stably determine corresponding perturbations in the source and reflectivity. The stability of this determination improves as the slowness aperture over which the data is defined increases. Further, the normal operator for the convolutional seismogram model is continuous with respect to velocity. Thus the stability result for constant background velocities may be extended to more realistic background velocity models which vary slowly and smoothly with depth. The theory above is illustrated with four synthetic numerical examples derived from marine data. The examples indicate that for a wide slowness aperture, inversion is very effective in establishing the true shape of the reflectivity and the shape and location of the compactly supported energy source. As this aperture window narrows, the corresponding inversion-estimated model still describes the data quite accurately, but the inversion is not able to recover the original two distinct parameters.

1 INTRODUCTION

In his 1954 thesis, Enders Robinson stated that "the seismic trace is the response of the system consisting of the earth and recording apparatus to the impulsive source, the explosion." Further, he said "in the final analysis one is interested in the various components of this total response; for example, one wishes to separate components of reflected energy from those of non-reflected energy" [1]. One of the most basic tasks in seismology (and the one which Robinson devoted much time to) is removal of the input energy source from the seismic data. In the last four decades, seismologists have devised numerous methods for estimating and removing the source from the seismic data.

Robinson, for example, suggested separating the "dynamic component" or wavelet shape from the "random components" (arrival times and strengths of the wavelets) in a method known today as predictive deconvolution. This method assumes the wavelet is minimum phase. Another technique for removing the energy source from the seismic data is homomorphic deconvolution. The seismic data is approximated by convolving the source wavelet with the impulse response. By Fourier transforming the data, the convolution becomes multiplication which is then replaced by addition when the log is taken. An assumed dichotomy of the frequency content between the source and reflectivity allows these quantities to be determined separately from the sum [2]. A third idea is to measure the direct wave and then try to figure the input energy source from this measurement [3].

In this paper we suggest using inversion to estimate the energy source at the same time the earth parameters are being estimated. In seismic inversion one chooses a physical model to describe the propagation of waves through the medium and attempts to improve the fit of the model to the given data by successively updating the parameters which characterize the model. The problem of determining the velocity and quasi-impulsive source via inversion is analyzed in papers by Bube et al. [4] and Sacks [5]. Lewis analyzed a similar problem. He assumed the earth is a constant density acoustic layered fluid with pressure measured at the earth's surface. The propagating waves are assumed to be plane waves and only primary reflections are recorded. He did not require the source to be impulsive but did require the background velocity in this linearized model to be constant. He showed that perturbations in the seismic data *stably* determine corresponding perturbations in

the source and reflectivity [6].

Starting from the same model Lewis used, we sought to relax the unrealistic assumption of a constant background velocity medium. We give a second proof of the stability result for constant background velocities and prove that the normal operator is continuous with respect to velocity. Thus for background velocities which vary slowly and smoothly with depth (i.e., are close to constant), changes in the source and reflectivity must cause proportional changes in the seismic data. The ability to separately determine the two parameters improves with increasing slowness aperture.

Section 2 of this paper details the mathematical model we consider. Section 3 provides the mathematical results, namely, a new proof of stability for the constant case and the theorem showing that the normal operator is continuous with respect to velocity. Finally, in section 4 we apply inversion to synthetic marine data generated with a variable background velocity model, estimating both the energy source and reflectivity functions. Four experiments are described. In each case the starting reflectivity is the same (zero) and the starting guess for the source is an isotropic Ricker wavelet with the correct peak frequency but incorrect temporal location. We use output least squares inversion to estimate the source and reflectivity. The four models differ in that the data for each successive experiment is defined over a smaller and smaller slowness aperture. In each case we are able to find parameters which allow the model to fit the data equally well. However, the original source and reflectivity parameters are only correctly recovered (including the time location of the source) when the data is defined over a sufficiently large slowness aperture.

2 MODEL AND PROBLEM SPECIFICATIONS

We model the earth as an acoustic fluid with constant density and depth-dependent variable sound velocity $c(z)$. The velocity is assumed to vary slowly on the scale of a seismic wavelength and to determine the kinematics of wave propagation. The short-scale heterogeneities are modeled by the relative perturbation in the velocity, or the reflectivity, $r(z) = \delta c(z)/c(z)$. The source is assumed to be isotropic and to have point support. The layered medium assumption above (that the velocity depends only on depth) allows us to apply the Radon integral transform (or plane-wave decomposition) to the normal displacement gotten from the solution to the acoustic wave equation. Thus one can reduce the three-dimensional problem to a family of one-dimensional equations [7]. These equations are parameterized by slowness, p. By assuming a primaries only or single-scattering approximation and by using high-frequency asymptotics, we can write the convolutional equation for the seismogram,

$$S(t,p) = f(t) * \tilde{r}(t,p)$$

.

Here, "$*$" denotes convolution in time t, and f is the isotropic source. The expression for the reflectivity as a function of time, $\tilde{r}$ (or perturbation of the Green's function for the acoustic wave equation) is given by $\tilde{r}(t,p) \approx \int dz[A(z)r(z,p)]\delta(t-2\tau)$ where A is the reflectivity amplitude from geometric optics. If v is the vertical (plane-wave) velocity, $v(z,p) = c(z)/\sqrt{1-c^2(z)p^2}$, we may write the travel-time function

$$\tau(z,p) = \int_0^z d\zeta \frac{1}{v(\zeta,p)}.$$

We shall also need the inverse of the travel-time function, which we denote by $z(t,p)$; thus

$\tau(z(t,p),p) = t$ and $z(\tau(\zeta,p),p) = \zeta$. This primaries-only, plane-wave, layered medium, constant density acoustic model is likely the simplest model of seismic wave propagation which one can use to describe real seismograms. For an example of its use in modeling seismic field data see the paper by Symes and Carazzone [8].

3 MATHEMATICAL RESULTS

3.1 Background

In his thesis, Lewis analyzed the effect of small perturbations in the source and reflectivity on the seismogram, in the case that the background velocity is constant [6]. From the plane-wave convolutional model for the seismogram, we may write the perturbed seismogram as

$$\delta S(t,p) = \delta f(t) * \tilde{r}(t,p) + f(t) * \delta\tilde{r}(t,p). \tag{3.1}$$

Lewis showed that the perturbed seismogram determines both the perturbation in the source and the perturbation in the reflectivity uniquely. For instance, if the perturbation in the data is equal to zero, then the perturbations in both the source and reflectivity must also be identically zero. Obvious nonuniqueness due to scale ambiguities between the two parameters (source and reflectivity) is ruled out by an added constraint which fixes the scale of one of the two quantities.

Further, he showed that perturbations in the seismic data *stably* determine corresponding perturbations in the source and reflectivity. This determination for source perturbations is valid within the passband of the source itself. Similarly, determination of reflectivity perturbations is constrained to a corresponding spatial frequency passband for the reflectivity. The stability improves as the range of slowness values increases. Conversely, as the range is reduced to a single trace, the ability to separately determine the perturbations in the source and reflectivity simultaneously is lost. The numerical examples in section 4 show that although it may be easy to find model parameters which explain a small aperture (or single trace) set of data, these parameters will not necessarily be the ones which generated the data originally.

As is realistic, in this work Lewis assumed that both the source and reflectivity have compact support in time. Thus, the source cannot mathematically be truly band-limited. It is reasonable, however, to assume that outside of some frequency band the source has small enough contribution to be considered negligible and ignored [9].

In an effort to generalize the above result to the case in which the background velocity need not be constant, we have arrived at a new proof of Lewis' result (Theorem 3.1 below). We show in Theorem 3.2 that the normal operator corresponding to the convolutional forward model for the seismogram is continuous in the velocity. Thus, having established stability at one point in velocity model space, namely for constant background velocity media, the continuity result implies that in a small neighborhood of this point (i.e., for background velocities which don't stray too far from constant), the seismic data stably determines corresponding perturbations in the source and reflectivity.

3.2 Theory

Given the nature of the statistical deconvolution theory as described in the introduction, it is hardly surprising that a measure of "whiteness" turns up in the stability result to follow. For an interval $[\zeta_{\min}, \zeta_{\max}] \subset \mathbb{R}$ and $0 < \Delta\zeta < \zeta_{\max} - \zeta_{\min}$, define for $r \in L^2(\mathbb{R}), \mathrm{r} \neq 0$

$$W(\zeta_{\min}, \zeta_{\max}, \Delta\zeta; r) = \tag{3.2}$$

$$\inf \left\{ \frac{\frac{1}{\zeta_+ - \zeta_-} \int_{\zeta_-}^{\zeta_+} |\hat{r}|^2}{\|r\|^2_{L^2(\mathbb{R})}} : \zeta_{\min} \le \zeta_- < \zeta_+ \le \zeta_{\max} \, , \, \frac{1}{2}\Delta\zeta \le \zeta_+ - \zeta_- \le \Delta\zeta \right\}$$

That is, W measures the uniformity of distribution of Fourier components averaged over frequency intervals of length roughly $\Delta\zeta$. Note that $W > 0$ for any r of compact support. Evidently if f (and perhaps r) are band-limited, it is only possible to determine band-limited information about $\delta f, \delta r$ from the perturbational relation 3.1. For $\eta > 0$, we define an *η-passband* for $f \in L^2(\mathbb{R})$ to be a symmetric frequency interval $[-\omega_{\max}, -\omega_{min}] \cup [\omega_{min}, \omega_{\max}]$ over which

$$|\omega \hat{f}(\omega)| \ge \eta \|f\|_{L^2(\mathbb{R})} \tag{3.3}$$

Theorem 1 *Suppose that $0 \le p_{\min} \le p_{\max}$, $0 < \omega_{min} < \omega_{\max}$, $\eta > 0$, and $\Omega_f = [-\omega_{\max}, -\omega_{min}] \cup [\omega_{min}, \omega_{\max}]$ is an η-passband for $f \in L^2[0,T]$. Fix the size of the source, i.e., $\|\hat{f}\|_{L^2(\Omega_f)} = 1$. Suppose also that $r \in L^2[0,Z]$. Then for any $\delta f \in L^2[0,T]$ which satisfies*

$$\int_{\Omega_f} d\omega \overline{\widehat{\delta f}}(\omega) \hat{f}(\omega) = 0 \tag{3.4}$$

and $\delta r \in L^2[0,Z]$,

$$\left\| \widehat{\delta f} \right\|_{L^2(\Omega_f)} + \left\| \widehat{\delta \tilde{r}} \right\|_{L^2(\Omega_f \times [p_{\min}, p_{\max}])} \le K \, \|\delta S\|_{L^2([0,T] \times [p_{\min}, p_{\max}])}$$

where K depends on $p_{\min}, p_{\max}, c, \omega_{min}, \omega_{\max}, \eta$, and

$$W := W\left(\frac{\omega_{min}}{v(p_{\max})}, \frac{\omega_{\max}}{v(p_{\min})}, \frac{\omega_{min}}{2}\left(1 + \frac{v(p_{\max})}{v(p_{\min})}\right); r \right)$$

Proof. Set $v(p) = v(z,p) = (c^{-2} - p^2)^{-\frac{1}{2}}$. Then $\hat{\tilde{r}}(\omega, p) = v(p)\hat{r}\,(\omega / v(p))$. Write $\zeta(\omega, p) = \omega / v(p)$. Then Fourier transformation of the expression for δS (expression 3.1) and a little algebra yield

$$\frac{\overline{\hat{r}}(\zeta)}{v(p)} \frac{\widehat{\delta S}(\omega, p)}{\hat{f}(\omega)} = \left[\frac{\widehat{\delta f}(\omega)}{\hat{f}(\omega)} \right] |\hat{r}(\zeta)|^2 + \overline{\hat{r}}(\zeta) \widehat{\delta r}(\zeta) \tag{3.5}$$

The map $p \to \zeta(\omega, p)$ is smooth and invertible. Viewed as an identity in ω and ζ, expression 3.5 holds over the ζ interval $[\zeta_{\min}(\omega), \zeta_{\max}(\omega)]$, where $\zeta_{\min}(\omega) = \omega / v(p_{\max})$, and $\zeta_{\max}(\omega) = \omega / v(p_{\min})$. A calculation shows that

$$[\zeta_{\min}(\sigma\omega), \zeta_{\max}(\omega)] \subset \quad [\zeta_{\min}(\omega), \zeta_{\max}(\omega)] \cap [\zeta_{\min}(\sigma\omega), \zeta_{\max}(\sigma\omega)] \tag{3.6}$$

if $1 \le \sigma \le \frac{1}{2}\left(1 + \frac{v(p_{\max})}{v(p_{\min})}\right)$. Therefore we can subtract equation 3.5 at the point $\sigma\omega$ from the same expression at the point ω so long as ζ remains in the range $\zeta \in [\zeta_{\min}(\sigma\omega), \zeta_{\max}(\omega)]$. We obtain

$$\overline{\hat{r}}(\zeta)\left[\frac{\widehat{\delta S}(\omega, p(\omega,\zeta))}{\hat{f}(\omega)v(p(\omega,\zeta))} - \frac{\widehat{\delta S}(\sigma\omega, p(\sigma\omega,\zeta))}{\hat{f}(\sigma\omega)v(p(\sigma\omega,\zeta))}\right] = \left[\frac{\widehat{\delta f}(\omega)}{\hat{f}(\omega)} - \frac{\widehat{\delta f}(\sigma\omega)}{\hat{f}(\sigma\omega)}\right]|\hat{r}(\zeta)|^2 \tag{3.7}$$

Integrate both sides of 3.7 to get

$$\left|\frac{\widehat{\delta f}(\omega)}{\hat{f}(\omega)} - \frac{\widehat{\delta f}(\sigma\omega)}{\hat{f}(\sigma\omega)}\right| = \left|\left(\int_{\zeta_{\min}(\sigma\omega)}^{\zeta_{\max}(\omega)} d\zeta\ |\hat{r}(\zeta)|^2\right)^{-1} \int_{\zeta_{\min}(\sigma\omega)}^{\zeta_{\max}(\omega)} d\zeta\ \overline{\hat{r}}(\zeta)\left[\frac{\widehat{\delta S}(\omega, p(\omega,\zeta))}{\hat{f}(\omega)v(p(\omega,\zeta))} - \frac{\widehat{\delta S}(\sigma\omega, p(\sigma\omega,\zeta))}{\hat{f}(\sigma\omega)v(p(\sigma\omega,\zeta))}\right]\right|$$

$$\le \frac{K}{\eta W \|r\|_{L^2[0,Z]}}\left[\left(\int_{p_{\min}}^{p_{\max}} dp|\widehat{\delta S}(\omega,p)|^2\right)^{\frac{1}{2}} + \left(\int_{p_{\min}}^{p_{\max}} dp\ |\widehat{\delta S}(\sigma\omega,p)|^2\right)^{\frac{1}{2}}\right]$$

$$\le \frac{K}{\eta W \|r\|_{L^2[0,Z]}}\|\delta S\|_{L^2([0,T]\times[p_{\min},p_{\max}])}$$

Here we have used the "passband" and "whiteness" hypotheses 3.2 and 3.3. K stands for a quantity depending only on c, $p_{\min}$, and $p_{\max}$, which may vary from expression to expression. Denote by N the smallest integer greater than

$$\frac{\omega_{\max} - \omega_{min}}{\frac{1}{2}\left(1 + \frac{v(p_{\max})}{v(p_{\min})}\right)}$$

Then for any $\omega \in [\omega_{min}, \omega_{\max}]$

$$\left|\frac{\widehat{\delta f}(\omega)}{\hat{f}(\omega)} - \frac{\widehat{\delta f}(\omega_{min})}{\hat{f}(\omega_{min})}\right| = \left|\sum_{n=1}^{N} \frac{\widehat{\delta f}(\sigma^n\omega_{min})}{\hat{f}(\sigma^n\omega_{min})} - \frac{\widehat{\delta f}(\sigma^{n-1}\omega_{min})}{\hat{f}(\sigma^{n-1}\omega_{min})}\right|$$

$$\le \frac{NK}{\eta W \|r\|_{L^2[0,Z]}}\|\delta S\|_{L^2([0,T])\times[p_{\min}p_{\max}])}$$

Evidently the same inequality holds for the negative part of the passband Ω_f, with ω_{min} replaced by $-\omega_{min}$. Set $k = \widehat{\delta f}(\omega_{min})/\hat{f}(\omega_{min})$. Because $\widehat{\delta f}$ is orthogonal to $\hat{f}$ over Ω_f,

$$\left\|\widehat{\delta f}\right\|^2_{L^2(\Omega_f)} = \int_{\Omega_f} d\omega\ \overline{\widehat{\delta f}}(\omega)\left(\widehat{\delta f}(\omega) - k\hat{f}(\omega)\right)$$

$$= \int_{\omega_{min}}^{\omega_{\max}} d\omega\ \overline{\widehat{\delta f}}(\omega)\hat{f}(\omega)\left(\frac{\widehat{\delta f}(\omega)}{\hat{f}(\omega)} - \frac{\widehat{\delta f}(\omega_{min})}{\hat{f}(\omega_{min})}\right) + \int_{-\omega_{\max}}^{-\omega_{min}} d\omega\ \overline{\widehat{\delta f}}(\omega)\hat{f}(\omega)\left(\frac{\widehat{\delta f}(\omega)}{\hat{f}(\omega)} - \frac{\widehat{\delta f}(\omega_{min})}{\hat{f}(\omega_{min})}\right)$$

$$\le \left\|\widehat{\delta f}\right\|_{L^2(\Omega_f)}\left\|\hat{f}\right\|_{L^2(\Omega_f)}\frac{NK}{\eta W\ \|r\|_{L^2[0,Z]}}\|\delta S\|_{L^2([0,T]\times[p_{\min},p_{\max}])}$$

which establishes the required bound for $\widehat{\delta f}$. The corresponding bound for $\delta\tilde{r}$ follows from the definition of δS and the passband inequality 3.3.

□

Corollary 1 *For any spatial frequency interval (ζ_-, ζ_+) contained in the interior of*

$$\left[\frac{-\omega_{\max}}{v(p_{\min})}, \frac{-\omega_{min}}{v(p_{\max})}\right] \bigcup \left[\frac{\omega_{min}}{v(p_{\max})}, \frac{\omega_{\max}}{v(p_{\min})}\right] ,$$

there exists a constant $K(\zeta_-, \zeta_+)$ depending also on the quantities mentioned in the theorem, so that

$$\left\|\widehat{\delta r}\right\|_{L^2[\zeta_-,\zeta_+]} \leq K \left\|\delta S\right\|_{L^2([0,T]\times[p_{\min},p_{\max}])}$$

Note. The constant K in the corollary is not uniform in ζ_-, ζ_+ but depends on the size of the neighborhood of $[\zeta_-, \zeta_+]$ contained in the band defined above.

Theorem 2 *The conclusion of Theorem 1 continues to hold, under the same hypotheses, for $c \in C^1[0, Z]$, provided that $\|dc/dz\|_{C^0[0,Z]}$ is sufficiently small. Specifically, there exist $\sigma, K > 0$ depending on the same quantities as in the statement of Theorem 1 so that*

$$\left\|\frac{dc}{dz}\right\|_{C^0[0,Z]} \leq \sigma$$

implies that for arbitrary $\delta f \in L^2[0, T]$, $\delta r \in L^2[0, Z]$,

$$\left\|\widehat{\delta f}\right\|_{L^2(\Omega_f)} + \left\|\widehat{\delta\tilde{r}}\right\|_{L^2(\Omega_f\times[p_{\min},p_{\max}])} \leq K \left\|\delta S\right\|_{L^2(\mathbb{R}\times[p_{\min},p_{\max}])}$$

Proof. Evidently, the assertion of the theorem boils down to a statement about

$$\|\delta S\|^2_{L^2(R\times[p_{\min},p_{\max}])} = \left\langle \begin{pmatrix} \delta f \\ \delta r \end{pmatrix}, N \begin{pmatrix} \delta f \\ \delta r \end{pmatrix} \right\rangle_{L^2[0,T]\times L^2[0,Z]}$$

where N is the *normal operator*.

Explicitly,

$$N \begin{pmatrix} \delta f \\ \delta r \end{pmatrix} = \begin{pmatrix} N_{rr}\delta f + N_{fr}\delta r \\ N_{rf}\delta f + N_{ff}\delta r \end{pmatrix}$$

where

$$\begin{aligned}
N_{rr}\delta f(t) &= \int_{p_{\min}}^{p_{\max}} p dp \int ds_1 \int ds_2 \; r(z(s_1,p))\; r(z(s_2,p))\; \delta f(t+s_1-s_2) \\
N_{fr}\delta r(t) &= \int_{p_{\min}}^{p_{\max}} p dp \int ds_1 \int ds_2 \; f(s_1)\; r(z(s_2,p))\; \delta r(z(t+s_1-s_2,p)) \\
N_{rf}\delta f(z) &= \int_{p_{\min}}^{p_{\max}} p dp \frac{1}{v(z,p)} \int ds_1 \int ds_2 \; f(s_1)\; r(z(s_2,p))\; \delta f(\tau(z,p)+s_1-s_2) \\
N_{ff}\delta r(z) &= \int_{p_{\min}}^{p_{\max}} p dp \frac{1}{v(z,p)} \int ds_1 \int ds_2 \; f(s_1)\; f(s_2)\; \delta r(z(\tau(z,p)+s_1-s_2,p))
\end{aligned}$$

$N = N[c]$ is a self-adjoint operator on the Hilbert space $L^2[0,T] \times L^2[0,Z]$ for each positive smooth velocity profile $c(z)$. We will show that N is *continuous* in c, in an appropriate sense. Then the conclusion of the theorem will follow from the perturbation theory of bounded self-adjoint operators [10]. All four components of N may be treated the same way, so we show the calculations explicitly only for N_{rf}. Denote by $N^0_{rf} = N_{rf}[c(0)]$ the operator N_{rf} for the constant velocity $c \equiv c(0)$. Then a change of variables of integration yields

$$\left(N_{rf}\,\delta f - N^0_{rf}\delta f\right)(z) = \int_{p_{\min}}^{p_{\max}} p dp \left\{ \frac{1}{v(z,p)} \int\int dz_1 ds\; r(z_1)\,\delta f(s) f(s + \tau(z_1,p) - \tau(z,p)) \right.$$

$$\left. - \frac{1}{v_0(p)} \int\int dz_1 ds\; r(z_1)\,\delta f(s) f(s + \tau_0(z_1,p) - \tau_0(z,p)) \right\}$$

where the zero subscripts denote quantities associated with the constant velocity $c(0)$. This last is

$$= \int_{p_{\min}}^{p_{\max}} p dp \left\{ \left(\frac{1}{v(z,p)} - \frac{1}{v_0(p)} \right) \int\int dz_1 ds r(z_1)\,\delta f(s)\; f(s + \tau(z_1,p) - \tau(z,p)) \right.$$

$$\left. + \frac{1}{v_0(p)} \int\int dz_1 ds r(z_1) \delta f(s) \left[f(s + \tau(z_1,p) - \tau(z,p)) - f(s + \tau_0(z_1,p) - \tau_0(z,p)) \right] \right\}$$

Now

$$\begin{aligned} & f(s + \tau(z_1,p) - \tau(z,p)) - f(s + \tau_0(z_1,p) - \tau_0(z,p)) \\ &= \int_s^{s + (\tau(z_1,p) - \tau(z,p)) - (\tau_0(z_1,p) - \tau_0(z,p))} d\sigma f'(\sigma + \tau_0(z_1,p) - \tau_0(z,p)) \\ &= -\frac{1}{(z - z_1) v_0(p) p} \left\{ \frac{\partial}{\partial p} \int_s^{s + (\tau(z_1,p) - \tau(z,p)) - (\tau_0(z_1,p) - \tau_0(z,p))} d\sigma f(\sigma + \tau_0(z_1,p) - \tau_0(z,p)) \right\} \\ &\quad + \left(\int_z^{z_1} dz' p(v(z',p) - v_0(p)) \right) f(s + \tau(z_1,p) - \tau(z,p)) \end{aligned}$$

Substituting this last expression into the integral and integrating by parts with respect to p, we obtain a lengthy expansion for the kernel of the Hilbert-Schmidt operator N_{rf}, each term in which consists of

1. a factor of $r(z_1)$
2. either $f(\cdot)$ or $\frac{1}{z - z_1} \int_I f$, where the interval of integration I has length $= O(|z - z_1|)$
3. a coefficient function of z, z_1 and p which is uniformly bounded by a function of $p_{\min}, p_{\max}$ and $\|c - c(0)\|_{C^1[0,Z]}$

hence in turn by $\|dc/dz\|_{C^0[0,Z]}$. Thus the Hilbert-Schmidt norm, or $N_{rf} - N^0_{rf}$ is bounded by

$$K \|r\|_{L^2[0,Z]} \|f\|_{L^2[0,T]} \left\| \frac{dc}{dz} \right\|_{C^0[0,Z]}$$

where K is a function of $Z, \|c\|_{C^1[0,Z]}$, $p_{\min}$, and $p_{\max}$.

The other three components may be treated the same way, so

$$\left\| N - N^0 \right\| \leq K \left\| r \right\|_{L^2[0,Z]} \left\| f \right\|_{L^2[0,T]} \left\| \frac{dc}{dz} \right\|_{C^0[0,Z]}$$

Now the key conclusion of Theorem 3.1 may be expressed as:

$$N^0 \geq \begin{pmatrix} \varepsilon E_{\Omega f} & 0 \\ 0 & 0 \end{pmatrix}$$

where $\varepsilon > 0$ and $E_{\Omega f}$ is the operator of Fourier transformation (of f), followed by multiplication by the bandpass filter (1 inside Ωf, 0 outside), followed by the inverse Fourier transform. The continuity estimate above now implies the same bound for N:

$$N \geq \begin{pmatrix} \varepsilon E_{\Omega f} & 0 \\ 0 & 0 \end{pmatrix}$$

where ε is uniform over $\left\| f \right\|_{L^2[0,T]} = 1$ and L^2-bounded sets of $r \in L^2[0, Z]$ subject to the "pseudowhiteness" constraint expressed in Theorem 3.1. Thus the result has been proved for the δf term, and the complete conclusion of Theorem 3.2 follows from the normal equations as before.

□

To summarize, we have shown that perturbations in the source and reflectivity functions are both well-determined by the corresponding perturbations of the seismogram, within their passbands, so long as the rate of change of velocity with depth is sufficiently small, and so long as the reference reflectivity has a "whiteness" property. These conditions are merely sufficient for "well-posedness within the passband" of the linearized problem. Their necessity is far from obvious. Moreover, our results imply only that a reasonable misfit criterion, suitably regularized, will be convex near the global minimizer for noise-free data. In particular our result says little directly about the global behavior of misfit functions or algorithms to minimize them.

4 A NUMERICAL EXAMPLE

To test the theoretical results discussed above numerically, we performed experiments on synthetic data generated from real data. The examples shown here were based on data provided by Exxon Production Research Company. All tests were done on a Sun Sparcstation 2 using the Differential Semblance Optimization package, a seismic simulation and inversion code under development at Rice University.

We began with one common-midpoint data gather taken from a marine seismic survey. The Radon transform was applied to yield 48 plane-wave traces with slowness values ranging from $p_{min} = .1158$ ms/m to $p_{max} = .36468$ ms/m. We were also given an estimate of the anisotropic air gun source in the form of a 31-term Legendre expansion in slowness. The coefficients in the series were functions of time only.

The procedure used to generate the target model for our experiment was the following. The target isotropic source is the first term of the 31-term source estimate (which represents the isotropic component of the air gun source). This isotropic source has been filtered to have a peak frequency of roughly 15 Hz and a peak in time at 110 ms. To generate a realistic target reflectivity, we inverted the plane-wave field data for the reflectivity using an inversion-estimated background velocity. The output of the (least squares) inversion was an estimate of the reflectivity (the relative perturbation in the velocity in this case).

For the experiments reported here (in each case, determination of both the source and reflectivity) we chose the variable background velocity shown in Figure 1. We generated four new sets of data (each with a different slowness aperture) for our synthetic experiments using the reflectivity from the field data inversion as input. The seismic data was also filtered by the 15 Hz Ricker wavelet and consisted of 13 traces each of about 3 seconds time duration.

We successively updated the source and reflectivity estimates by minimizing the mean squared difference between the actual data and the data predicted by our model (*O*utput *L*east *S*quares inversion). The method we used (coordinate search or alternation) requires the source parameters be fixed, and the reflectivities estimated by output least squares inversion. Then the reflectivities are updated and held fixed and the source parameters estimated by OLS inversion. The source is updated and this cycle is repeated until convergence [11].

Alternation, although notoriously inefficient, is attractive for initial experiments because it requires only successive solution of simple linear least-squares problems. Obviously, quasi-Newton methods could be applied to the problem and would likely reduce the number of iterations dramatically.

The initial estimate of the reflectivity used for the inversions was $r = 0$. For the initial source estimate, we chose a Ricker wavelet also with peak frequency of 15 Hz but which had its peak centered in time at 0 ms (Figure 2). The source location was of interest to us in this experiment. In practice, one might reasonably expect to be able to estimate the power spectrum of the source. However, one would not expect to be able to guess at the location of the peak in time (i.e., the phase). Each inversion round included an estimation of the source and an estimation of the reflectivity.

In experiment 1 we attempted to find source and reflectivity parameters to explain the data shown in Figure 3(a). This synthetic data was generated with the full slowness aperture range of the original plane wave data, namely from $p_{min} = .1158$ ms/m to $p_{max} = .36468$ ms/m. The seismogram used in experiment 2 is shown in Figure 4(a). For this experiment, the slowness interval between consecutive traces was cut in half, but the total number of traces remained the same . The resulting aperture range was from $p_{min} = .1158$ ms/m to $p_{max} = .2402$ ms/m. The slowness interval between neighboring traces was halved once more for experiment 3, yielding a slowness range from $p_{min} = .1158$ ms/m to $p_{max} = .1780$ ms/m. The corresponding data is displayed in Figure 5(a). Finally, a slowness interval of 0 ms/m was used, i.e., all thirteen traces in experiment 4 were the same. The data to be matched is the single-trace seismogram of Figure 6(a).

Figures 3(b), 4(b), 5(b), and 6(b) display the target isotropic source (dashed line) and an inversion-estimated source (solid line) from the corresponding data (3(a), 4(a), 5(a), and 6(a) respectively). Similarly, figures 3(c), 4(c), 5(c), and 6(c) display the target reflectivity (dashed line) and estimated reflectivity (solid line) for each experiment. Recall that using the convolutional model for the seismogram and determining both the source and reflectivity, a scale ambiguity exists (which is why we fix the size of the source function in the theoretical results). Thus, one may scale the source up by a constant α and the reflectivity down by the constant $1/\alpha$ and fit the data equally as well as one would without the scaling. Multiplication by the constant -1 is, of course, allowed as well. Thus, in each experiment, the graphs were designed to show the best results for that case (which may have included polarity reversal). In experiments 1 and 2, the source and reflectivity inversion results were scaled by a factor of -1, whereas in experiments 3 and 4 they were not. The inversion estimates plotted for the four different experiments correspond to the point at which the inversion-estimated source and reflectivity had reduced the root mean squared error to 7% of the data norm. Each time we narrowed the slowness aperture, the convergence rate for the alternation algorithm progressively worsened. For example, to reduce the error to 7% took only eighteen rounds of alternation with the full aperture range of data (experiment 1). The

half aperture range (experiment 2) took forty rounds; and finally, in experiment 3, one-hundred and fifty rounds of alternation were required to reduce the rms error to 7% of the data norm. The degenerate case of data with only a single trace converged to less than 10% error in only two rounds of alternation. We note, however, that the experiments with a wider range of slowness values allow determination of the reflectivity and correctly locate the source peak at 110 ms. As the slowness range narrows, the inversion scheme is no longer able to move the initial source guess to its target location, although the fit to data is comparable across experiments. The ability to separately determine the two parameters has been lost.

5 CONCLUSION

In order to estimate the mechanical parameters which describe a section of the subsurface, seismologists must take into account the energy they introduce into the ground as an imaging device. Rather than removing the energy source from the data, one can invert for this source while simultaneously estimating the earth parameters. In this paper we examine a simple seismogram model, namely the plane-wave convolutional model derived from the constant density, variable sound velocity acoustic wave equation. We invert for the energy source and a high-frequency perturbation of the velocity (or reflectivity). Theoretically we find that for slowly varying background velocities, the corresponding seismic data stably determines perturbations in the source and reflectivity. Numerically we describe four inversion experiments performed on synthetic data generated from real marine data. The initial source guess was located at the time origin whereas the true source was peaked at 110ms. Although we are able to determine both parameters quite accurately for data defined over a wide range of slownesses, as this range narrows to the single trace limit, we can no longer separately recover the original source (and its correct time location) and the reflectivity.

6 ACKNOWLEDGEMENTS

This work was partially supported by the National Science Foundation, the Office of Naval Research, the Texas Geophysical Parallel Computation Project, the Schlumberger Foundation, and The Rice Inversion Project. TRIP Sponsors for 1994 are Advance Geophysical, Amoco Production Co., Conoco Inc., Cray Research Inc., Discovery Bay Co., Exxon Production Research Co., Interactive Network Technologies, Mobil Research and Development Corp., and Texaco Inc.

References

[1] E.A. ROBINSON. Predictive decomposition of seismic traces. *Geophysics*, 22:767–778, 1957.

[2] T.J. ULRYCH. Application of homomorphic deconvolution to seismology. *Geophysics*, 36:650–660, 1971.

[3] A. ZIOLKOWSKI. *Deconvolution*. International Human Resources Development Corporation, Boston, 1984.

[4] K. BUBE, P. LAILLY, P. SACKS, F. SANTOSA, and W.W. SYMES. Simultaneous determination of source wavelet and velocity profile using impulsive point-source data from a layered fluid. *Geophys. J.*, 95:449–462, 1988.

[5] P.E. SACKS. A velocity inversion problem involving an unknown source. *SIAM J. Appl. Math.*, 50(3):931–941, 1990.

[6] R.M. LEWIS. *Source-Velocity Identification for a Layered Model of Reflection Seismology*. PhD thesis, Department of Mathematical Sciences, Rice University, Houston, Texas, U.S.A, 1989.

[7] S. TREITEL, P.R. GUTOWSKI, and D.E. WAGNER. Plane-wave decomposition of seismograms. *Geophysics*, 47:1375–1401, 1982.

[8] W.W. SYMES and J. CARAZZONE. Velocity inversion by differential semblance optimization. *Geophysics*, 56(5):654–663, 1991.

[9] D. SLEPIAN. Some comments on fourier analysis, uncertainty and modeling. *SIAM Review*, 25(3):379–393, 1983.

[10] T. KATO. *Perturbation Theory for Linear Operators*. Springer, New York, 1966.

[11] S.E. MINKOFF and W.W. SYMES. Simultaneous determination of the source-time function and reflectivity via inversion. In *Proc. 63rd Annual International Meeting*, pages 649–652, Washington, D.C., U.S.A., 1993. Society of Exploration Geophysicists. Expanded abstract.

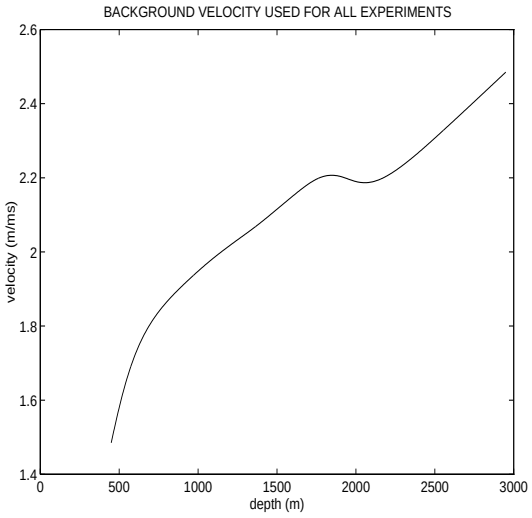

FIGURE 1: Variable background velocity model used to generate the seismic data shown in Figures 3(a), 4(a), 5(a), and 6(a).

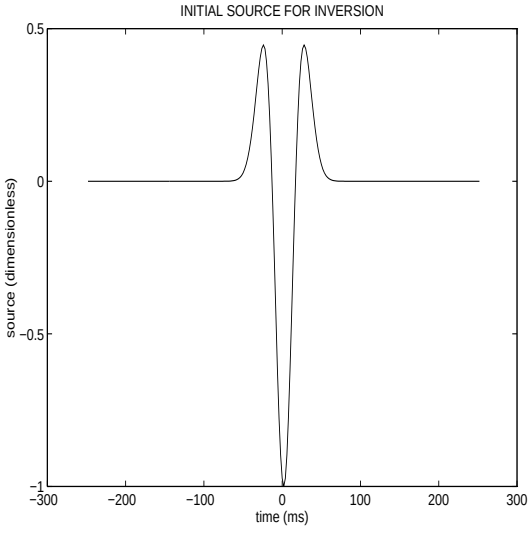

FIGURE 2: Initial guess for the source, an inverted 15 Hz Ricker wavelet centered at 0 ms.

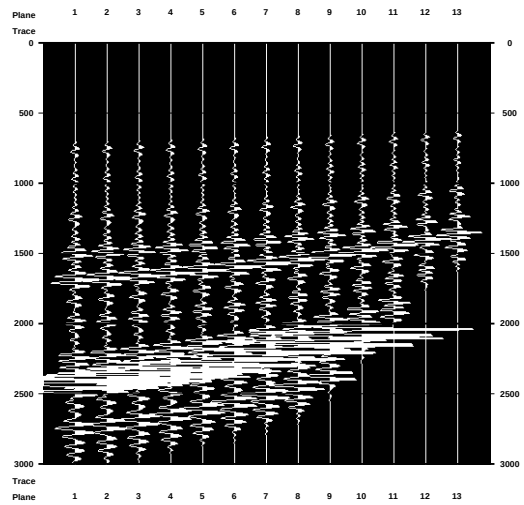

FIGURE 3(a): Seismic data generated from the variable background velocity shown in Figure 1 and the isotropic source in Figure 3(b) (dashed line). The slowness aperture for the data is p_{min} = .1158 ms/m to p_{max} = .36468 ms/m.

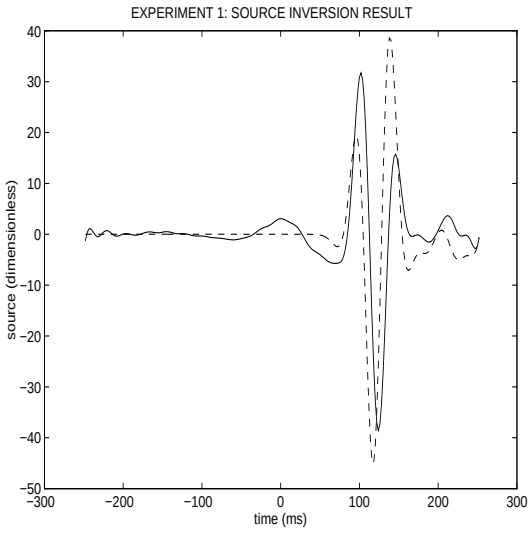

FIGURE 3(b): Source inversion result at alternation round 18 for the data shown in Figure 3(a). The rms error/data norm = 7.5%. Solid line: estimated source (scaled). Dashed line: target source.

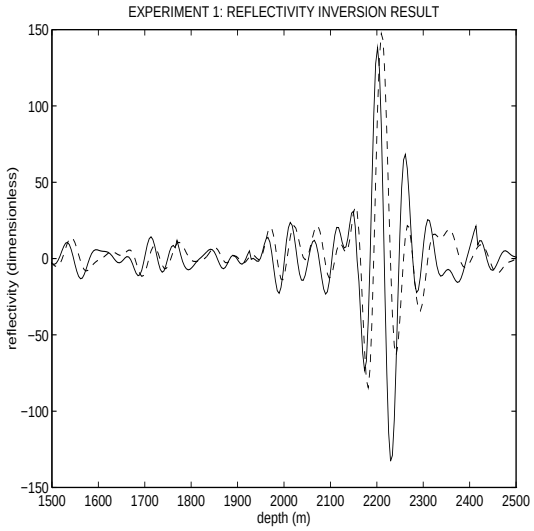

FIGURE 3(c): Reflectivity inversion result at alternation round 18 for the data shown in Figure 3(a). The rms error/data norm = 7%. Solid line: estimated reflectivity (scaled). Dashed line: target reflectivity.

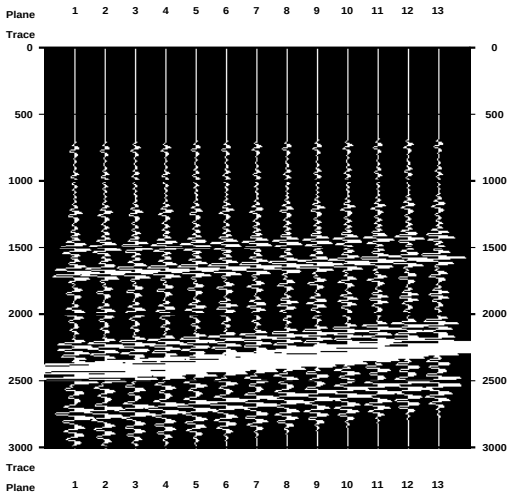

FIGURE 4(a): Seismic data generated from the variable background velocity shown in Figure 1 and the isotropic source in Figure 4(b) (dashed line). The slowness aperture for the data is p_{min} = .1158 ms/m to p_{max} = .2402 ms/m.

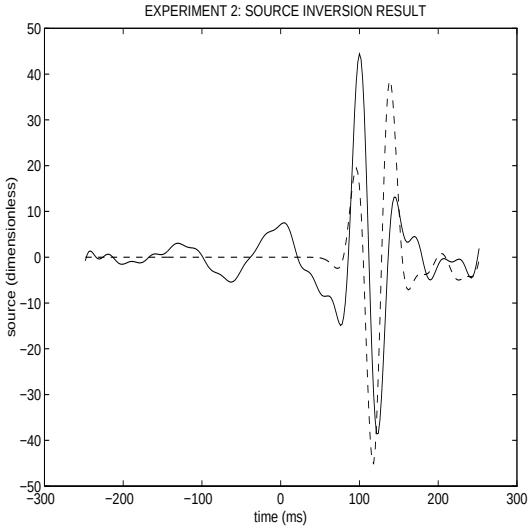

FIGURE 4(b): Source inversion result at alternation round 40 for the data shown in Figure 4(a). The rms error/data norm = 7%. Solid line: estimated source (scaled). Dashed line: target source.

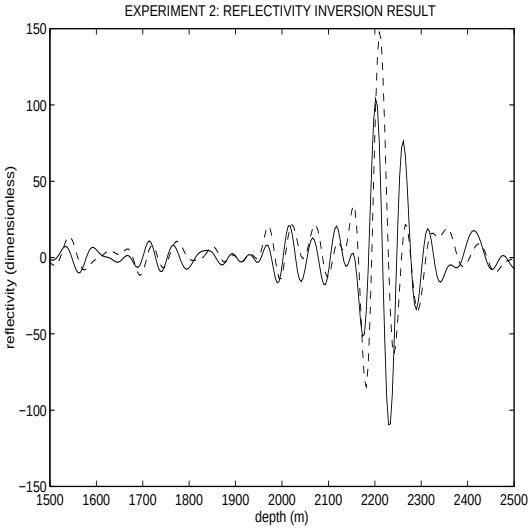

FIGURE 4(c): Reflectivity inversion result at alternation round 40 for the data shown in Figure 4(a). The rms error/data norm = 7%. Solid line: estimated reflectivity (scaled). Dashed line: target reflectivity.

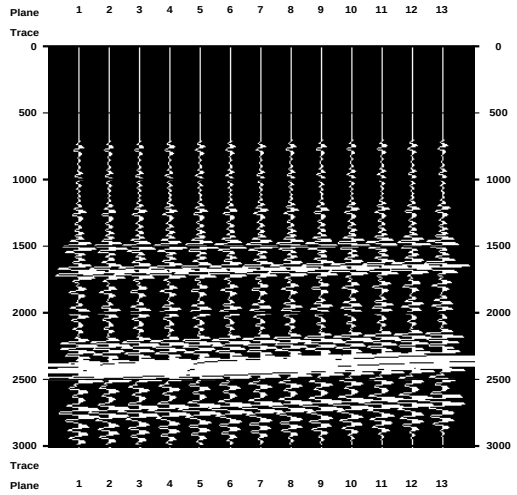

FIGURE 5(a): Seismic data generated from the variable background velocity shown in Figure 1 and the isotropic source in Figure 5(b) (dashed line). The slowness aperture for the data is p_{min} = .1158 ms/m to p_{max} = .1780 ms/m.

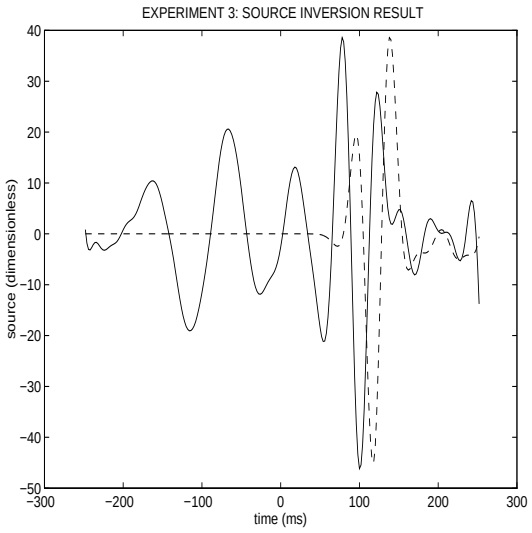

FIGURE 5(b): Source inversion result at alternation round 150 for the data shown in Figure 5(a). The rms error/data norm = 7%. Solid line: estimated source (scaled). Dashed line: target source.

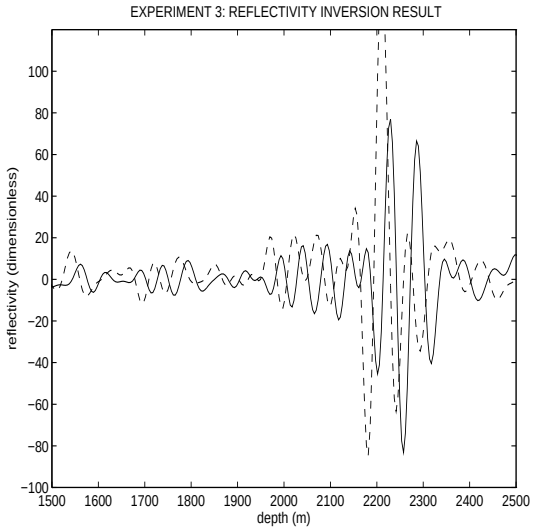

FIGURE 5(c): Reflectivity inversion result at alternation round 150 for the data shown in Figure 5(a). The rms error/data norm = 7%. Solid line: estimated reflectivity (scaled). Dashed line: target reflectivity.

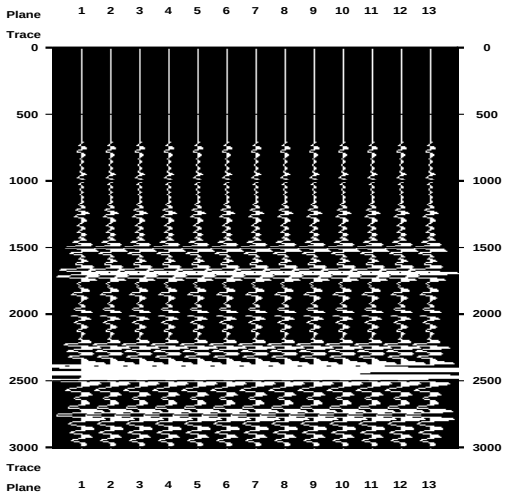

FIGURE 6(a): Seismic data generated from the variable background velocity shown in Figure 1 and the isotropic source in Figure 6(b) (dashed line). The slowness aperture for the data is $p_{min} = p_{max} = .1158$ ms/m (i.e., all thirteen records are the same).

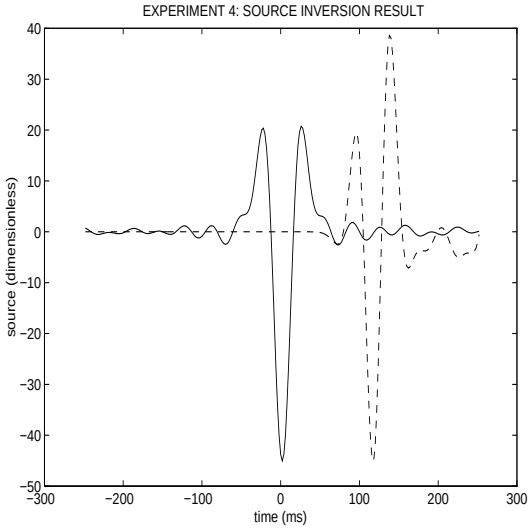

FIGURE 6(b): Source inversion result at alternation round 2 for the data shown in Figure 6(a). The rms error/data norm = 9%. Solid line: estimated source (scaled). Dashed line: target source.

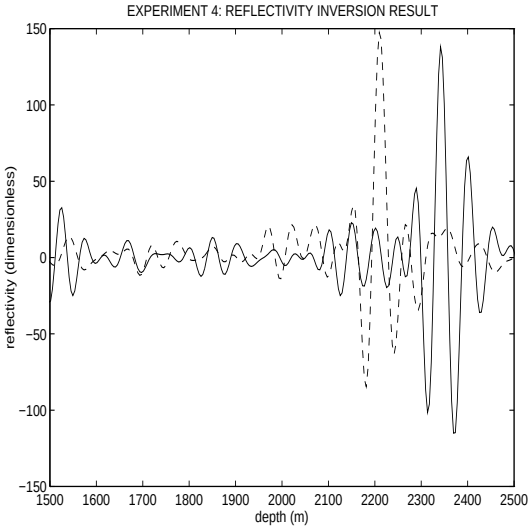

FIGURE 6(c): Reflectivity inversion result at alternation round 2 for the data shown in Figure 6(a). The rms error/data norm = 5%. Solid line: estimated reflectivity (scaled). Dashed line: target reflectivity.